Water-water correlations in electrolyte solutions probed by hyper-Rayleigh scattering

David P. Shelton[a)]
Department of Physics and Astronomy, University of Nevada, Las Vegas, Nevada 89154-4002, USA

(Received 1 August 2017; accepted 17 November 2017; published online 7 December 2017)

Long-range ion-induced correlations between water molecules have been observed by second-harmonic or hyper-Rayleigh scattering experiments with conflicting results. The most recent work observed a large difference between the results for H_2O and D_2O, and large discrepancies with the previously proposed theory. However, the present observations are in quantitative agreement with the model where the ion electric field induces second harmonic generation by the water molecules, and ion-ion correlations given by the Debye-Huckel theory account for intensity saturation at high ion concentration. This work compares experimental results with theory and addresses the apparent discrepancies with previous experiments. *Published by AIP Publishing.* https://doi.org/10.1063/1.4998589

I. INTRODUCTION

Second-harmonic or hyper-Rayleigh scattering (HRS) is a nonlinear light scattering technique widely used to measure the first hyperpolarizability β of molecules in solution,[1,2] and HRS has largely replaced the previous alternative electric-field-induced second harmonic generation (ESHG or EFISH) technique.[3] It is usually assumed that only incoherent scattering from the individual molecules contributes to HRS. However, for electrolyte solutions, there is a coherent ESHG contribution to the HRS signal due to the orientation correlations induced by the electric field of the ions in solution.[4] The ion-induced HRS intensity increases with ion concentration and saturates at high ionic strength due to the spatial correlations of the ions, as described by the Debye-Huckel theory.

In this model for ion-induced HRS,[4] the radial electric field of an ion induces a radial orientation of the surrounding water molecular dipoles which decreases as r^{-2} with distance r from the ion. This weak induced radial orientation of the molecules produces scattered field contributions that add coherently with a sum that increases with r until it is limited by phase differences when $Kr > \pi$, where K is the magnitude of the scattering wave vector. Most of the ion-induced HRS signal comes from many weakly oriented molecules at large distances $r > \pi/K$.[5] At low ion concentration, the ion positions are uncorrelated, so the scattered fields induced by each ion add incoherently and the ion-induced HRS intensity is proportional to ion concentration. At high ion concentration, the Debye-Huckel ion-ion spatial correlations[6] cause destructive interference of the scattered fields induced by the individual ions and the ion-induced HRS intensity reaches a limiting value at high ion concentration. At small distances compared to the separation of the ions, the ion-field-induced orientation distribution of the water dipole vectors is radial, and at larger distances, it is a random vector field with only longitudinal spatial Fourier components.[4,7]

Previous measurements of the intensity of the ion-induced HRS contribution for KCl–D_2O solutions did not quantitatively agree with the theoretical predictions of this model,[4] and more recent measurements for several electrolyte solutions find even larger differences between theory and experiment for the ion-induced HRS intensity and its ion concentration dependence.[8] These recent experiments also find dramatic differences between the results measured for electrolyte solutions with H_2O and D_2O.[8] These discrepancies have motivated a number of subsequent investigations.[9,10] Quantitative understanding of ion-induced HRS is relevant to second harmonic generation (SHG) from aqueous interfaces since the bulk SHG can interfere with the surface contribution and because ion-induced HRS probes the electric field induced effects that are modeled in surface and interface studies.[11–13]

In this work, the ion-induced HRS contribution has been re-measured for solutions of KCl in H_2O and D_2O. The ionic strength dependence of ion-induced HRS is found to be nearly identical for H_2O and D_2O and is in quantitative agreement with the predictions of the Debye-Huckel theory. There is also quantitative agreement between theory and experiment for the intensity of ion-induced HRS, when the orientation correlations in pure water are taken into account. In the following, the experimental methods and results will be presented and analyzed, and an attempt will be made to reconcile the present results with the previous observations.

II. HRS EXPERIMENT

The HRS experimental apparatus and methods are similar to those previously employed[4,5,14–19] and are described and discussed in detail in Ref. 14. Linearly polarized pulses from an Nd:YAG (yttrium aluminium garnet) laser (operating at λ_0 = 1064 nm, 4.3 kHz repetition rate, 100 ns pulse duration) are focused to a 4.5 μm beam waist radius in the liquid sample in a standard square 10 mm fluorimeter cuvette. Scattered light at $\theta_s = 90°$ is collected and collimated by an aspheric lens (f = 13.8 mm), analyzed by a linear polarizer, focused into an optical fiber, and fiber-coupled to a 60 cm^{-1} spectral filter

[a)]shelton@physics.unlv.edu

[532 nm center, 2 nm transmission bandwidth, full width at half maximum (FWHM)] followed by the photon counting detector measuring the integrated intensity. The laser beam average power was P_{av} = 2.5 W for D_2O but was reduced to 0.75 W for H_2O due to absorption and thermal defocusing of the laser beam by the sample. The experiments were done with multi-longitudinal mode laser output (0.6 cm^{-1} FWHM) to increase the HRS signal. Several measurements were also made using a wider spectral filter (536 nm center, 46 nm FWHM).

The water sample (H_2O, 18 MΩ cm, Millipore Milli-Q; D_2O, 99.9 at.% D, Sigma-Aldrich) was de-ionized by continuous flow in a closed loop containing a PTFE (polytetrafluoroethylene)-tube peristaltic pump, ion-exchange resin column (Dowex Monosphere MR-450 UPW), 0.2 μm PTFE filter, sample cell, conductivity cell, and reservoir, in that order. D_2O was exchanged for H_2O in the resin before loading the column used for the D_2O measurements. The column with 1 cm^3 of DI resin can maintain ionic strength 0.1 μM continuously for days or weeks in the 20 cm^3 circulating fluid volume. Samples with controlled larger ion concentration were obtained by adding concentrated KCl (99.98%, Baker) solution to the de-ionized circulating fluid, with the ion-exchange column by-passed. The temperature of the continuously circulating fluid was T = 25.0 °C, and the ion concentration was determined from the conductivity recorded before and after each HRS measurement, assuming that H^+, OH^- (or D^+, OD^-), K^+, and Cl^- are the only ions present.[20–22] The conductivity sensor was calibrated with 3 mM and 10 mM KCl–H_2O solutions.[22]

Contamination by ions desorbed from the walls of the loop is minimized by using the DI column to remove all ions but H^+ and OH^- (or D^+ and OD^-), adding KCl, and completing the HRS measurement before significant contamination could occur. Ionic strength determined from the sample conductivity may have a systematic error if the desorbed ions have mobility or charge different from that of K^+ and Cl^-. Desorption rate about 2 μM/h was estimated from the conductivity increase of the circulating liquid after closing the DI column. Several H_2O data points in Fig. 1 at low KCl concentration have larger error bars as a result of low HRS signal for H_2O and short measurement time to avoid errors due to desorbed ions.

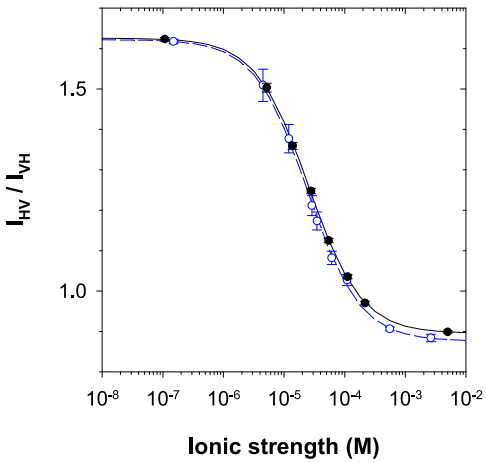

FIG. 1. HRS intensity ratio I_{HV}/I_{VH} measured with a 2 nm spectral filter for water at T = 298 K as a function of ionic strength. The solid black curve is Eq. (1) fit to the D_2O data (solid black circles) and the dashed blue curve is the fit to the H_2O data (open blue circles), with fit parameters given in Table II.

Scattering configurations with incident and scattered light polarized either perpendicular or parallel to the horizontal scattering plane are denoted VV, HV, VH, and HH, where V denotes vertical polarization, H denotes horizontal polarization, and the first and second letters refer to the incident and scattered light, respectively. Ratios of HRS intensities were measured (I_{VV}/I_{HV} and I_{HV}/I_{VH}).[14] The effect of intensity drift was cancelled by using several hundred alternate 10 s measurements of the two polarization configurations for each ratio. Rapid switching between polarization configurations was enabled using a liquid crystal variable wave plate (LCVWP) to control the laser polarization and a fast rotator[15] to control the analyzing polarizer for the scattered light. The collection numerical aperture ($NA = n \sin\theta$) was controlled by a circular aperture following the collection lens, and the HRS intensity ratio at NA = 0 was obtained by extrapolating measurements in the range $0.07 < NA < 0.15$ to zero collection aperture with a fit function $a + b\,(NA)^2$.[14] HRS intensity I_{VV} corrected for thermal lensing[23] due to 7% (0.8%) absorption[24,25] of the input laser beam by the H_2O (D_2O) sample was obtained from the P = 0 limit of S_{VV}/P^2, where S_{VV} is the HRS signal measured with laser power P. Thermal lensing has no effect on the HRS intensity ratio measurements.

III. EXPERIMENTAL RESULTS

The main results of this experiment are the values of I_{HV}/I_{VH} measured for KCl–H_2O and KCl–D_2O solutions as a function of ionic strength $c = (1/2)\sum_i Z_i^2 \rho_i$, where Z_i is the charge and ρ_i is the concentration of ion species i. The results of these measurements are shown in Table I and Fig. 1. The curves fit to the data points in Fig. 1 have the form

$$I_{HV}/I_{VH} = A/[1 + Bx/(1 + x)], \quad (1)$$

where $x = c/c_0$, $A = (I_{HV}/I_{VH})_{c=0}$ and $B = (I^i_{VH})_{c\to\infty}/(I_{VH})_{c=0} = I^i_{VH,\infty}/I_{VH,0}$. The fit coefficients c_0, A, and B are given in Table II. Equation (1) is the ratio of HRS intensity I_{HV}, which is independent of ion concentration, and $I_{VH} = I_{VH,0} + I^i_{VH}$, which has an ion-induced contribution I^i_{VH} that saturates at high ion concentration. The reason for measuring the ratio I_{HV}/I_{VH} is that I_{HV} serves as an ion-independent internal

TABLE I. HRS intensity ratio I_{HV}/I_{VH} measured with a 2 nm spectral filter for water at T = 298 K as a function of ionic strength c. Numbers in parentheses are the uncertainties in the last digits.

H_2O		D_2O	
c (M)	I_{HV}/I_{VH}	c (M)	I_{HV}/I_{VH}
1.49×10^{-7}	1.618(5)	1.07×10^{-7}	1.623(4)
4.48×10^{-6}	1.509(40)	5.16×10^{-6}	1.503(11)
1.19×10^{-5}	1.377(35)	1.38×10^{-5}	1.359(8)
2.87×10^{-5}	1.211(24)	2.77×10^{-5}	1.248(7)
3.48×10^{-5}	1.174(22)	5.40×10^{-5}	1.125(5)
6.07×10^{-5}	1.082(16)	1.11×10^{-4}	1.036(5)
1.08×10^{-4}	1.027(14)	2.16×10^{-4}	0.970(5)
5.52×10^{-4}	0.907(5)	5.01×10^{-3}	0.899(3)
2.63×10^{-3}	0.884(9)		

TABLE II. Coefficients A, B, c_0 for the fit of Eq. (1) to the HRS intensity ratio I_{HV}/I_{VH} data in Table I and Fig. 1.

	H_2O	D_2O
A	1.622 ± 0.003	1.626 ± 0.003
B	0.851 ± 0.006	0.816 ± 0.005
c_0 (μM)	44.7 ± 1.7	45.7 ± 0.9

TABLE III. HRS intensity ratios for water at T = 298 K using 2 nm and 46 nm spectral filters. The estimate for B is reduced for the wider filter. The hyper-Raman band intensity ratios in the last two lines are obtained using the differences between filters.

	H_2O	D_2O
2 nm filter		
I_{VV}/I_{HV}	7.06 ± 0.02	7.41 ± 0.01
$I_{HV}/I_{VH,0}$	1.622 ± 0.003	1.626 ± 0.003
$I_{VV}/I_{VV}(D_2O)$	0.82 ± 0.02	
46 nm filter		
I_{VV}/I_{HV}	5.71 ± 0.06	6.19 ± 0.02
I_{HV}/I_{VH}	1.06 ± 0.01	1.139 ± 0.003
I_{VV}/I_{VV}(2 nm)	1.374 ± 0.016	1.298 ± 0.010
I_{HV}/I_{HV}(2 nm)	1.70 ± 0.03	1.55 ± 0.01
I_{VH}/I_{VH}(2 nm)	2.59 ± 0.05	2.22 ± 0.02
B	0.328 ± 0.007	0.368 ± 0.004
Difference		
I_{VV}/I_{HV}	3.8 ± 0.2	4.0 ± 0.2
I_{HV}/I_{VH}	0.71 ± 0.04	0.74 ± 0.02

reference for the measurements of the ion concentration dependent intensity I_{VH}, producing more accurate results for the ion-induced HRS contribution I^i_{VH}. Figure 1 shows that Eq. (1) is a good fit to the HRS data, and that the HRS results for H_2O and D_2O are nearly the same.

The HRS intensity I_{VV} and polarization ratio I_{VV}/I_{HV} were also measured and are slightly different for H_2O and D_2O.

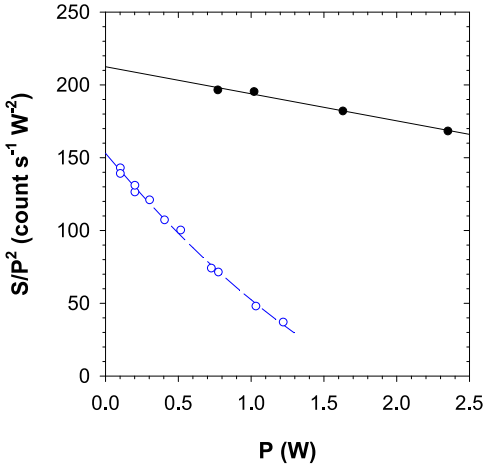

FIG. 2. Normalized HRS signal S_{VV}/P^2 measured for D_2O (solid black circles) and H_2O (open blue circles) with a 2 nm spectral filter at T = 298 K. The normalized signal decreases with laser beam power P due to the thermal lens effect and is extrapolated to P = 0 using the function $a(1 + bP + cP^2)$ fit to the data. The solid black curve is the fit to the D_2O data with a = 213 ± 2 count s^{-1} W^{-2}, b = −0.088 ± 0.007 W^{-1}, c = 0 W^{-2}, and the dashed blue curve is the fit to the H_2O data with a = 153 ± 2 count s^{-1} W^{-2}, b = −0.78 ± 0.06 W^{-1}, c = 0.12 ± 0.04 W^{-2}.

Results for I_{VV}/I_{HV}, and the result for $I_{VV}(H_2O)/I_{VV}(D_2O)$, are given in Table III. The $I_{VV}(H_2O)/I_{VV}(D_2O)$ result accounts for both absorption and the thermal lensing effect shown in Fig. 2. These HRS measurements were made with a 2 nm spectral filter and de-ionized samples but are insensitive to dissolved ions. The intensities I_{VV}, I_{HV}, and I_{VH} for de-ionized H_2O (0.2 μM) and D_2O (0.1 μM) were also measured using a 46 nm spectral filter. The intensity measured with the wider filter is larger due to inclusion of the 660 cm^{-1} (460 cm^{-1}) libration mode hyper-Raman band.[26–28] The measurements made using 2 nm and 46 nm filters were combined to also determine the ratios I_{VV}/I_{HV} and I_{HV}/I_{VH} for this hyper-Raman band, with the results given in Table III. The ratio $I_{HV}/I_{VH} < 1$ indicates that this is a longitudinal collective mode.[29]

IV. COMPARISON WITH THEORY

Expressions for c_0 and B, quantifying the concentration dependence and intensity of ion-induced HRS, were previously derived.[4] [In the notation of Ref. 4, $c_0 = Z^2\rho_D$ and $B = (S/B)_\infty$.] The expression for c_0 is

$$c_0 = \frac{K^2\varepsilon_0\varepsilon_s k_B T}{2e^2}, \tag{2}$$

where K is the magnitude of the scattering wave vector, ε_0 is the vacuum permittivity, ε_s is the static relative dielectric constant,[30] k_B is the Boltzmann constant, and e is the electronic charge. The scattering wave number K for HRS at $\theta_s = 90°$ is[19]

$$K^2 = (4\pi/\lambda_0)^2(n_i^2 + n_s^2), \tag{3}$$

where λ_0 is the vacuum wavelength of the incident light and n_i and n_s are refractive indices at the incident and scattered light frequencies.[25,31–33] Table IV gives data needed to evaluate Eqs. (2) and (3) and the resulting values for c_0. The difference between the experimental and theoretical results for c_0 in Tables II and IV is insignificant, −0.9 ± 1.7 μM for H_2O and 0.7 ± 0.9 μM for D_2O.

The expression for B from Ref. 4 is

$$B_1 = \frac{\rho_s f(0)^2 k_B T}{2\varepsilon_0\varepsilon_s}\frac{[\gamma_\perp + \mu_0\beta_\perp/(3k_BT)]^2}{\langle\beta^2_{XZZ}\rangle}$$
$$= \frac{f(0)^2 y}{2\varepsilon_s}\frac{\beta_\perp^2}{\langle\beta^2_{ZXX}\rangle}\left[1 + \frac{3k_BT\gamma_\perp}{\mu_0\beta_\perp}\right]^2, \tag{4}$$

where ρ_s is the number density of solvent molecules,[21] μ_0 is the permanent dipole moment,[34] β and γ are the molecular first and second hyperpolarizabilities,[35] $f(0) = \varepsilon_s(\varepsilon_\infty + 2)/$

TABLE IV. Molecular parameters ε_s, n_{1064}, and n_{532} for water at T = 298 K used with Eqs. (2) and (3) to calculate the ionic strength parameter c_0.

Parameter	H_2O	D_2O
ε_s	78.45[a]	78.08[a]
n_{1064}	1.3240[b]	1.3211[b]
n_{532}	1.3349[c]	1.3296[c]
$2\pi/K$ (nm)	283.0	283.8
c_0 (μM)	45.60	45.11

[a]Reference 30.
[b]Reference 31.
[c]References 25, 32, and 33.

$(\varepsilon_\infty + 2\varepsilon_s)$ is the Onsager local field factor with ε_∞ being the high frequency dielectric constant,[36] $y = \rho_s \mu_0^2/(9\varepsilon_0 k_B T)$ is the dimensionless dipole strength, and the isotropic average $\langle \beta_{ZXX}^2 \rangle$ gives the HRS intensity for a pure liquid with uncorrelated randomly oriented molecules. Far from resonance or in the static limit, where the tensors $\beta_{\alpha\beta\gamma}$ and $\gamma_{\alpha\beta\gamma\delta}$ are invariant under all permutations of the indices (Kleinman symmetry), one has[37–40]

$$\beta_\perp = \frac{1}{3}\beta_{||} = \frac{1}{5}\sum_\xi \beta_{z\xi\xi}, \tag{5}$$

$$\gamma_\perp = \frac{1}{3}\gamma_{||} = \frac{1}{15}\sum_{\xi\eta} \gamma_{\xi\xi\eta\eta}, \tag{6}$$

$$\langle \beta_{ZZZ}^2 \rangle = \frac{9}{45}|\beta^{(1)}|^2 + \frac{6}{105}|\beta^{(3)}|^2, \tag{7}$$

$$\langle \beta_{XZZ}^2 \rangle = \langle \beta_{ZXX}^2 \rangle = \frac{1}{45}|\beta^{(1)}|^2 + \frac{4}{105}|\beta^{(3)}|^2. \tag{8}$$

For molecules that also have C_{2v} symmetry, one has

$$|\beta^{(1)}|^2 = \frac{3}{5}(\beta_{zzz} + \beta_{zyy} + \beta_{zxx})^2 = 15\beta_\perp^2, \tag{9}$$

$$|\beta^{(3)}|^2 = \frac{1}{10}(3\beta_{zzz} - 2\beta_{zyy} - 2\beta_{zxx})^2 + \frac{3}{2}(\beta_{zyy} - \beta_{zxx})^2. \tag{10}$$

In the case that $\gamma_\perp$ can be neglected, and $|\beta^{(3)}| = 0$ so that $\beta_\perp^2 / \langle \beta_{ZXX}^2 \rangle = 3$, Eq. (4) becomes

$$B_0 = 3f(0)^2 y/(2\varepsilon_s), \tag{11}$$

which is the simplest approximate estimate for B. Evaluating Eq. (11) using the data in Table V gives B_0 which is about twice the experimentally measured value for B in Table II. Also in this approximation, $I_{VV}/I_{HV} = \langle \beta_{ZZZ} \rangle / \langle \beta_{XZZ} \rangle = 9$ and $I_{HV}/I_{VH,0} = \langle \beta_{XZZ} \rangle / \langle \beta_{ZXX} \rangle = 1$.

An improved theoretical estimate for B makes use of the hyperpolarizability tensor components given in Table VI, calculated in Ref. 35 for molecules in liquid water. This is an *ab initio* calculation at the Moller-Plesset MP2 level of theory, for the static hyperpolarizability of the water molecule in a local environment with a strong axial field and symmetric (model II) or asymmetric (model III) field gradient. The effect of the local environment is to induce an increment $\Delta\beta$ large enough to reverse the sign of β (with respect to the dipole).

TABLE V. Molecular parameters for water at $T = 298$ K used to calculate $y = \rho_s \mu_0^2/(9\varepsilon_0 k_B T)$ and the simplest ion-induced HRS estimate $B_0 = 3f(0)^2 y/(2\varepsilon_s)$ from Eq. (11).

	H_2O	D_2O
ρ_s (M)	55.34[a]	55.15[a]
μ_0 (D)	2.95[b]	
ε_s	78.45[c]	78.08[c]
ε_∞	4.49[d]	
$f(0)$	3.155	3.154
y	9.838	9.802
B_0	1.872	1.874

[a]Reference 22.
[b]Reference 34.
[c]Reference 30.
[d]Reference 36.

TABLE VI. Molecular hyperpolarizabilities (atomic units) for liquid H_2O from Ref. 35 used with Eq. (4) to calculate the improved ion-induced HRS estimate $B_1 = I^i_{VH,\infty}/I_{VH,0}$.

	Model II	Model III
β_{zxx}	4.3	5.7
β_{zyy}	31.7	10.9
β_{zzz}	31.2	31.6
$\beta_\perp$	13.44	9.64
$\gamma_\perp$	887	892
$3k_B T\gamma_\perp/(\mu_0\beta_\perp)$	0.161	0.226
$\lvert\beta^{(1)}\rvert^2$	2710	1394
$\lvert\beta^{(3)}\rvert^2$	1334	58.5
$\langle \beta_{ZXX}^2 \rangle$	111.0	33.2
$\beta_\perp^2/\langle \beta_{ZXX}^2 \rangle$	1.627	2.799
I_{VV}/I_{HV}	5.57	8.50
$I_{HV}/I_{VH,0}$	1	1
B_1	1.368	2.625

The non-zero octupolar $|\beta^{(3)}|^2$ contribution reduces the value of $\beta_\perp^2/\langle \beta_{ZXX}^2 \rangle$, and non-zero $\gamma_\perp$ increases the last factor of Eq. (4). The values for B_1 in Table VI evaluated using the calculated hyperpolarizabilities are 1.6–3.1× the experimentally measured B value for H_2O in Table II. The discrepancy between theoretical and experimental values for B is smaller for model II. This model has a larger octupolar $|\beta^{(3)}|^2$ contribution and is also a better fit to the HRS data from Ref. 18 that is analyzed in Ref. 41.

The orientation correlation of molecules in the pure liquid, which enhances HRS due to the vector $\beta^{(1)}$ part of β, is neglected in Eq. (4). Including the transverse mode enhancement factor C_T, the HRS intensity $I_{VH,0}$ for the pure liquid is given by[19,41]

$$I_{VV} = \frac{9}{45}C_T|\beta^{(1)}|^2 + \frac{6}{105}|\beta^{(3)}|^2, \tag{12}$$

$$I_{HV} = \frac{1}{45}C_T|\beta^{(1)}|^2 + \frac{4}{105}|\beta^{(3)}|^2, \tag{13}$$

$$I_{VH,0} = \frac{1}{90}C_T|\beta^{(1)}|^2 + \frac{4}{105}|\beta^{(3)}|^2, \tag{14}$$

and the revised theoretical expression for B is

$$B_2 = \frac{f(0)^2 y}{2\varepsilon_s}\frac{\beta_\perp^2}{I_{VH,0}}\left[1 + \frac{3k_B T\gamma_\perp}{\mu_0\beta_\perp}\right]^2. \tag{15}$$

Table VII gives the values for $I_{VH,0}$ and B_2 calculated using Eqs. (14) and (15) with the hyperpolarizabilities from Ref. 35

TABLE VII. Molecular hyperpolarizabilities (atomic units) for liquid H_2O from Ref. 35 are used with Eq. (15) to calculate the ion-induced HRS contribution $B_2 = I^i_{VH,\infty}/I_{VH,0}$ including effects of orientation correlation in pure water, and B_3 which also includes collision-induced HRS.

	Model II	Model III
C_T	3.14	3.14
$I_{VH,0}/\langle \beta_{ZXX}^2 \rangle$	1.309	1.532
I_{VV}/I_{HV}	7.41	8.83
$I_{HV}/I_{VH,0}$	1.650	1.956
B_2	1.045	1.714
B_3	0.911	1.493

and C_T from Ref. 41. The values for B_2 in Table VII are 1.2–2.0× the experimentally measured B value for H_2O, and the values calculated for B_2, I_{VV}/I_{HV}, and $I_{HV}/I_{VH,0}$ increase as $|\beta^{(3)}|/|\beta^{(1)}|$ decreases going from model II to model III. The values for B_2, I_{VV}/I_{HV}, and $I_{HV}/I_{VH,0}$ obtained using model II differ from the experimental values by 23%, 5%, and 2%, respectively.

The final issue is the contribution of background signals included in the measured HRS intensity but not described by the expressions given above. Short range interactions during molecular collisions induce rapid fluctuations in the molecular hyperpolarizabilities and produce additional HRS with a broad spectrum. This collision-induced HRS accounts for the HRS observed from centro-symmetric molecules and is also present in the HRS spectra previously measured for D_2O.[42] The D_2O HRS spectrum at $T = 25\,^{\circ}C$ is the sum of two narrow Lorentzian functions (1.2 cm^{-1} FWHM), a broad Lorentzian (10.6 cm^{-1} FWHM) and a broad exponential function (70 cm^{-1}), where the integrated intensity of the broad components is 35% of the total HV intensity. Identifying the Lorentzian components as orientational HRS and the exponential component as collision-induced HRS, the fit functions from Ref. 42 were integrated over a 60 cm^{-1} band to determine the relative contributions of orientational and collision-induced HRS for the present HRS measurements. The collision-induced/orientational VH HRS intensity ratio obtained is 0.148. The effect of this additional spectral component is to reduce B_2 by the factor 0.871, giving the final estimates B_3 at the bottom of Table VII. The value of B_3 for model II differs from the experimental value by 7%.

V. PREVIOUS RESULTS

Ion-induced HRS was previously measured for KCl–D_2O solutions using nearly the same apparatus,[4] with the result $c_0 = 40 \pm 8$ μM, in agreement with the present result, and $B = 0.667 \pm 0.008$, significantly lower than the present result. In those experiments, the ion-induced contribution was determined from high resolution VH HRS spectra obtained using a Fabry-Perot interferometer. The ion-induced HRS peak spectral width increases with ion concentration and reaches 100 MHz at the highest ion concentration in those experiments, which is comparable to the 750 MHz free-spectral range of the interferometer. For solutions with the highest ion concentration and largest peak width, the background contribution estimated from the fit to the data becomes sensitive to the assumed shape for the wings of the spectral peak. This is due to overlap of successive orders of the Fabry-Perot transmission function, and the systematic error introduced by this effect could account for the 20% difference between the previous and present results for B.

The results of the other recent ion-induced HRS measurements[8] differ much more from the present work. The results from Ref. 8 for H_2O are $c_0 = 55 \pm 5$ μM and $B = 0.30 \pm 0.03$, and for D_2O they are $c_0 = 310 \pm 71$ μM and $B = 0.09 \pm 0.03$ [however $I_{VV}(H_2O)/I_{VV}(D_2O) = 0.8$ in Fig. S4 of Ref. 8 agrees with the result 0.82 ± 0.02 in Table III]. Those experiments measured the ratio of HRS intensities for electrolyte solutions and pure solvent samples, for solutions of H_2O with 21 different electrolytes and solutions of D_2O with NaCl. A 50 nm wide spectral filter was used, and the filter pass band (500-550 nm, $-540 < \Delta\nu < 1270$ cm^{-1} down-shift $\Delta\nu$ from the hyper-Rayleigh peak at 514 nm) includes both the hyper-Rayleigh band and the intermolecular libration hyper-Raman band (at 660 cm^{-1} in H_2O and 460 cm^{-1} in D_2O).[26–28] Including the hyper-Raman band increases $I_{VH,0}$ and reduces the measured value for B. The effect of the wide filter can be estimated from the results of the present experiment using the 46 nm wide filter (pass band $-690 < \Delta\nu < 920$ cm^{-1}) which also includes the hyper-Raman band. The factor by which $I_{VH,0}$ is increased and B is decreased is given by $I_{VH}/I_{VH}(2\,nm)$ in Table III. Dividing B in Table II by this factor gives the value for B in Table III.

Accounting for the wider pass band, the results for H_2O from Ref. 8 are in fair agreement with c_0 in Table II and B in Table III, with differences 10 ± 5 μM and 0.03 ± 0.03, respectively. The results for D_2O still do not agree with differences for c_0 and B that are 4× and 9× the stated uncertainties. Excess ions due to contamination of the nominally pure D_2O solvent could explain the results for D_2O in Ref. 8. If the sample and reference are both contaminated, then a larger additional ion concentration is required for a significant change in the sample/reference intensity ratio, and the maximum change is reduced. The predicted effect of 100 μM ionic contamination would be to reduce the maximum change to 0.09, with half-maximum change at 145 μM so that the differences between predicted and observed c_0 and B would be 165 ± 71 μM and 0.00 ± 0.03, respectively. Since the ion concentration was not measured *in situ*, such contamination is not ruled out.

VI. SUMMARY AND CONCLUSION

In summary, the theoretical predictions for c_0 are in very good agreement with the present experimental results for H_2O and D_2O, with no adjustable or uncertain parameters entering the theoretical calculation. The ionic strength dependence for ion-induced HRS is nearly the same for H_2O and D_2O, and the calculated results using the Debye-Huckel theory are quantitatively accurate. The agreement between experiment and theory is not as good for the ion-induced HRS intensity B, but in this case there is more uncertainty in the theoretical calculation. This calculation requires the first and second molecular hyperpolarizability tensor components and orientation correlation functions for the molecules in the liquid, and information about any additional spectral components in the region of interest. Not all the required data are available, definitive, and accurate. However, the difference between experiment and the final theoretical result B_3 with model II is small. This indicates that the present experimental results for H_2O, and also the observed differences between H_2O and D_2O, could be fit by the theory with small adjustments that are within the uncertainty of the model parameters. Not all the previous experimental results agree with the present results to within the stated uncertainties. However, the sources of the largest discrepancies have been identified and accounted for, and there are plausible explanations for the remaining apparent differences. All considered, the evidence indicates that the simple theoretical model for ion-induced HRS is correct and accurate.

ACKNOWLEDGMENTS

This work was supported by the National Science Foundation (NSF) through Grant No. CHE-1212114.

[1] J. Campo, F. Desmet, W. Wenseleers, and E. Goovaerts, Opt. Express **17**, 4587 (2009).
[2] K. Clays and A. Persoons, Phys. Rev. Lett. **66**, 2980 (1991).
[3] L.-T. Cheng, W. Tam, S. H. Stevenson, G. R. Meredith, G. Rikken, and S. R. Marder, J. Phys. Chem. **95**, 10631 (1991).
[4] D. P. Shelton, J. Chem. Phys. **130**, 114501 (2009).
[5] D. P. Shelton, J. Chem. Phys. **138**, 054502 (2013).
[6] J.-L. Barrat and J.-P. Hansen, *Basic Concepts for Simple and Complex Liquids* (Cambridge University Press, Cambridge, UK, 2003).
[7] D. P. Shelton, J. Chem. Phys. **143**, 134503 (2015); Erratum **146**, 199901 (2017).
[8] Y. Chen, H. I. Okur, N. Gomopoulos, C. Macias-Romero, P. S. Cremer, P. B. Petersen, G. Tocci, D. M. Wilkins, C. Liang, M. Ceriotti, and S. Roke, Sci. Adv. **2**, e1501891 (2016).
[9] D. M. Wilkins, D. E. Manolopoulos, S. Roke, and M. Ceriotti, J. Chem. Phys. **146**, 181103 (2017).
[10] C. Liang, G. Tocci, D. M. Wilkins, A. Grisafi, S. Roke, and M. Ceriotti, Phys. Rev. B **96**, 041407(R) (2017).
[11] G. Gonella, C. Lutgebaucks, A. G. F. de Beer, and S. Roke, J. Phys. Chem. C **120**, 9165 (2016).
[12] P. E. Ohno, S. A. Saslow, H.-F. Wang, F. M. Geiger, and K. B. Eisenthal, Nat. Commun. **7**, 13587 (2016).
[13] T. Joutsuka, T. Hirano, M. Sprik, and A. Morita, "Effects of third-order susceptibility in sum frequency generation spectra: A molecular dynamics study in liquid water," Phys. Chem. Chem. Phys. (published online).
[14] D. P. Shelton, Rev. Sci. Instrum. **82**, 113103 (2011).
[15] D. P. Shelton, W. M. O'Donnell, and J. L. Norton, Rev. Sci. Instrum. **82**, 036103 (2011).
[16] D. P. Shelton, J. Chem. Phys. **132**, 154506 (2010).
[17] D. P. Shelton, J. Chem. Phys. **136**, 044503 (2012).
[18] D. P. Shelton, J. Chem. Phys. **141**, 224506 (2014).
[19] D. P. Shelton, J. Chem. Phys. **144**, 234506 (2016).
[20] C. G. Swain and D. F. Evans, J. Am. Chem. Soc. **88**, 383 (1966).
[21] H. Weingartner and C. A. Chatzidimitriou-Dreismann, Nature **346**, 548 (1990).
[22] *CRC Handbook of Chemistry and Physics*, 68th ed., edited by R. C. Weast (CRC, Boca Raton, 1987).
[23] R. D. Pyatt and D. P. Shelton, J. Chem. Phys. **114**, 9938 (2001).
[24] K. F. Palmer and D. Williams, J. Opt. Soc. Am. **64**, 1107 (1974).
[25] S. Kedenburg, M. Vieweg, T. Gissibl, and H. Giessen, Opt. Mater. Express **2**, 1588 (2012).
[26] R. W. Terhune, P. D. Maker, and C. M. Savage, Phys. Rev. Lett. **14**, 681 (1965).
[27] C. Xu, J. B. Shear, and W. W. Webb, Anal. Chem. **69**, 1285 (1997).
[28] A. Maurice, Q. Ma, I. Russier-Antoine, E. Benichou, F. Canto, L. Couston, and P.-F. Brevet, Proc. SPIE **9171**, 91710S (2014).
[29] V. N. Denisov, B. N. Mavrin, and V. B. Podobedov, Phys. Rep. **151**, 1 (1987).
[30] K. R. Srinivasan and R. L. Kay, J. Chem. Phys. **60**, 3645 (1974).
[31] D. P. Shelton, Appl. Opt. **50**, 4091 (2011).
[32] M. Daimon and A. Masumura, Appl. Opt. **46**, 3811 (2007).
[33] H. Odhner and D. T. Jacobs, J. Chem. Eng. Data **57**, 166 (2012).
[34] A. V. Gubskaya and P. G. Kusalik, J. Chem. Phys. **117**, 5290 (2002).
[35] A. V. Gubskaya and P. G. Kusalik, Mol. Phys. **99**, 1107 (2001).
[36] J. Barthel, K. Bachhuber, R. Buchner, and H. Hetzenauer, Chem. Phys. Lett. **165**, 369 (1990).
[37] R. Bersohn, Y. Pao, and H. L. Frisch, J. Chem. Phys. **45**, 3184 (1966).
[38] P. D. Maker, Phys. Rev. A **1**, 923 (1970).
[39] D. P. Shelton and J. E. Rice, Chem. Rev. **94**, 3 (1994).
[40] D. P. Shelton, J. Chem. Phys. **137**, 044312 (2012); Erratum **146**, 209903 (2017).
[41] D. P. Shelton, J. Chem. Phys. **147**, 154501 (2017).
[42] D. P. Shelton, J. Chem. Phys. **117**, 9374 (2002); Erratum **121**, 3349 (2004).